

Freezing and large time scales induced by geometrical frustration

Michel Ferrero,¹ Federico Becca,¹ and Frédéric Mila²

¹ *INFN-Democritos, National Simulation Center, and SISSA, I-34014 Trieste, Italy.*

² *Institut de Physique Théorique, Université de Lausanne, CH-1015 Lausanne, Switzerland.*

(Dated: October 30, 2018)

We investigate the properties of an effective Hamiltonian with competing interactions involving spin and chirality variables, relevant for the description of the *trimerized* version of the spin-1/2 *kagome* antiferromagnet. Using classical Monte Carlo simulations, we show that remarkable behaviors develop at very low temperatures. Through an *order by disorder* mechanism, the low-energy states are characterized by a dynamical freezing of the chiralities, which decouples the lattice into “dimers” and “triangles” of antiferromagnetically coupled spins. Under the presence of an external magnetic field, the particular topology of the chiralities induces a very slow spin dynamics, reminiscent of what happens in ordinary spin glasses.

PACS numbers: 75.10.Nr, 75.10.Jm, 75.10.Hk

I. INTRODUCTION

The understanding and the characterization of the physical properties of frustrated magnetic systems is a central issue in modern theory of condensed matter. Indeed, in the last years, it has become evident that the magnetic interactions can give rise to a large variety of different unconventional phenomena, and that they can also be related to other phases of matter, like, for instance, superconductivity.

From an experimental point of view, an impressive number of materials with unconventional magnetic properties has been discovered, including quasi-one-dimensional and ladder systems,^{1,2} quasi-two-dimensional compounds with highly frustrated magnetic interactions,³ systems of weakly coupled dimers in various geometries,^{4,5,6,7} and fully three-dimensional frustrated systems based on corner sharing tetrahedra.⁸

A particular role in the list of frustrated magnetic systems is played by the magnetoplumbite $\text{SrCr}_{8-x}\text{Ga}_{4+x}\text{O}_{19}$, in which the anomalous magnetic properties are commonly attributed to planes of Cr^{3+} ions on the so-called *kagome* lattice, a lattice which can be described as a triangular lattice of triangles (see Fig. 1). In this compound, although a small quantity of disorder is present in the Chromium planes, there are evidences that the physical properties are not much affected by the presence of impurities. Nonetheless, linear-susceptibility measurements did not find any sign of conventional magnetic order down to $T \approx 4\text{K}$,⁹ despite a significant antiferromagnetic exchange coupling $J \approx 100\text{K}$ between Cr^{3+} ions, deduced from the Curie temperature. On the other hand, important insight into a possible spin-glass phase at very low temperatures comes from the non-linear susceptibility χ_3 measurements by Ramirez and collaborators.¹⁰ In usual spin-glass systems, it is known that $\chi_3^{-1} \approx (T - T_g)^\gamma$, where T_g is the spin-glass freezing temperature and γ is typically between 1 and 4.¹¹ In Ref. 10, it was found that χ_3 diverges at $T_g \approx 3.3\text{K}$, with $\gamma \approx 2$, indicating a possible freezing transition at this temperature. It is worth noting that the divergence

of χ_3 at a finite temperature indicates the importance of three-dimensional effects, since two-dimensional spin glasses are not expected to order at finite temperature.¹²

From a theoretical point of view, the possibility of a spin-glass behavior in the spin-1/2 Heisenberg model on the *kagome* lattice was suggested by Chandra and collaborators.¹³ The *kagome* lattice exhibits both frustration and a low coordination number, and, therefore, the Heisenberg antiferromagnet on the *kagome* lattice is a good candidate to find unconventional magnetic behaviors at very low temperature. The most problematic issue in the *kagome* antiferromagnet comes from the infinite number of classically degenerate ground states.¹⁴ As a consequence, the linear spin-wave spectrum of magnetic excitations possesses a whole branch of zero modes.¹⁵ Moreover, exact diagonalizations on finite-size systems have shown that the spin-spin correlations decrease very rapidly with distance.^{16,17,18} In addition, the series expansion from the Ising limit and high-temperature series point to the absence of magnetic order,^{19,20} whereas, according to large- N approaches, the ground state should be disordered with unbroken symmetry.²¹

The huge degeneracy of the classical ground states for the *kagome* antiferromagnet opens the possibility of the so-called *order by disorder* effect.²² Indeed, it is known that both thermal and quantum fluctuations can lift classical degeneracies in favor of particular states, which break some symmetry. Examples of this phenomenon are the ordering effect in the antiferromagnetic Ising model on the f.c.c. lattice due to thermal fluctuations²² or the establishment of a collinear order in the J_1-J_2 model due to quantum and thermal fluctuations.²³

In particular, thermal fluctuations could be effective to partially lift the classical ground state degeneracy by favoring states with largest entropy. In highly frustrated antiferromagnets, like the *kagome* lattice, the resulting energy landscape could still be very complicated, with many different “valleys” separated by high energy barriers, possibly giving the system a spin-glass behavior. In ordinary spin-glass materials, the disordered nature of the system gives rise to frustrated magnetic interactions

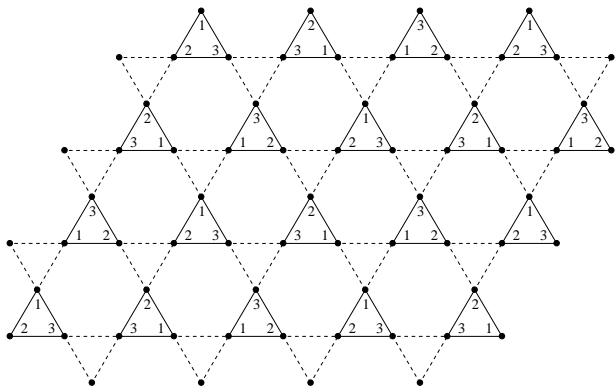


FIG. 1: The *trimerized kagome* lattice. The solid and dashed lines indicate the antiferromagnetic coupling J and J' , respectively. The numbers 1, 2 and 3 indicate the site indexing inside the elementary triangles which defines the gauge (see section II).

and, therefore, to many topologically different configurations that are energetically equivalent but separated by large (infinite) free energy barriers. The resulting physical properties show peculiar behaviors, with a very slow spin dynamics.^{24,25}

For the classical *kagome* model with full rotation symmetry in spin space, no evidence in favor of a spin-glass behavior could be found,^{14,26} and it seems that one has to go away from this very minimal model to have a chance to get a spin-glass-like behavior. Since $\text{SrCr}_{8-x}\text{Ga}_{4+x}\text{O}_{19}$ is made of spins $3/2$, it seems natural to turn to the quantum version of the model. In this paper, we consider an approximate way of including quantum fluctuations into a classical description. The starting point is the effective Hamiltonian obtained in Ref. 27 for the spin-1/2 Heisenberg model on a *trimerized kagome* lattice (see Fig. 1), which contains both spin and chirality variables. This is a modified version of the spin-1/2 Heisenberg model on the *kagome* lattice, in which the exchange couplings take two different values J and J' according to the pattern of Fig. 1. It is worth noting that this is actually the relevant case for the description of $\text{SrCr}_{8-x}\text{Ga}_{4+x}\text{O}_{19}$, since the presence of a triangular lattice between pairs of *kagome* layers leads to two kinds of bond lengths.

In Ref. 27, by using an appropriate mean-field approximation, this effective Hamiltonian has been useful to explain a number of important properties of the low-lying excitations of the *kagome* lattice, in particular the increase of the low-energy singlet states with the number of sites N like 1.15^N . Unfortunately, this effective Hamiltonian is far from being fully investigated because the interactions couple the spins and the chiralities in a non-trivial way. Nevertheless, given the very complicated nature of the problem, even at the classical level, the interplay between spins and chiralities can give rise to an unconventional behavior. In this respect, for any calculation in the true quantum case, it is very important

to know the underlying classical states, and, therefore, a first fundamental step is to establish the classical picture.

Recently, an interesting step toward the comprehension of the interplay between two different kinds of classical variables has been achieved by using a simple Ashkin-Teller model on a square lattice.²⁸ It was pointed out that the presence of two local degrees of freedom might be a key element to prevent any kind of long-range order and to obtain a very slow spin dynamics (reminiscent of a spin-glass-like behavior) at low-enough temperature. Hopefully, this finding can be seen as a first and crude explanation of the low-temperature behavior of $\text{SrCr}_{8-x}\text{Ga}_{4+x}\text{O}_{19}$, which does not show any magnetization down to very low temperature, but presents some promising evidence for a spin-glass behavior. It is also worth noting that, although in $\text{SrCr}_{8-x}\text{Ga}_{4+x}\text{O}_{19}$ the Cr^{3+} ions have spin $S = 3/2$, we consider the case treated in Ref. 27, suitable for $S = 1/2$.²⁹

In order to go beyond the simple model considered in Ref. 28, based on Ising variables, and to further clarify the possibility to obtain a spin-glass behavior in a more realistic system that does not contain explicit disorder but only frustration between two distinct local variables, we investigate the effective model of Ref. 27 in the classical limit.

The paper is organized as follows: In section II, we introduce the model, in section III we present the results for the case of zero external magnetic field, in section IV we present the results of the magnetization in the presence of an external magnetic field, and in section V we discuss the results and give our conclusions.

II. THE MODEL

Our starting point is the effective model obtained in Ref. 27 for the quantum spin-1/2 antiferromagnetic Heisenberg model on the *trimerized kagome* lattice. In this modified version of the usual spin-1/2 *kagome* antiferromagnet, the lattice is decomposed such as to emphasize the role of the elementary triangles building the *kagome* lattice. Indeed, the spins are coupled through two different constants J and J' as depicted in Fig. 1. In the limit $J'/J \ll 1$, the lattice can be seen as a triangular lattice of weakly coupled triangles and, by using ordinary perturbation theory, it is possible to derive an effective Hamiltonian in the subspace of the ground states of the triangles. The four-fold degenerate ground state of a triangle can be described by two spin-1/2 degrees of freedom, a spin $\vec{\sigma}$ and a chirality $\vec{\tau}$. With these variables, the effective Hamiltonian is defined on a triangular lattice of N sites and reads:²⁷

$$\begin{aligned} \mathcal{H}_0^{\text{eff}} &= J' \sum_{\langle i,j \rangle} \mathcal{H}_{ij}^{\sigma} \mathcal{H}_{ij}^{\tau}, \\ \mathcal{H}_{ij}^{\sigma} &= \vec{\sigma}_i \cdot \vec{\sigma}_j, \\ \mathcal{H}_{ij}^{\tau} &= \frac{1}{9} [1 - 2(\alpha_{ij} \tau_i^- + \alpha_{ij}^2 \tau_i^+)] [1 - 2(\beta_{ij} \tau_j^- + \beta_{ij}^2 \tau_j^+)], \end{aligned} \quad (1)$$

where $\sum'_{\langle i,j \rangle}$ denotes the sum over pairs of nearest-neighbor triangles. The complex parameters α_{ij} and β_{ij} depend on the type of bond: They take the values 1, ω or ω^2 [$\omega = \exp(2\pi i/3)$] when the original spins in triangles i and j involved in the bond (i,j) sit at site 1, 2 or 3 respectively, with the convention of Fig. 1. Note that we have the freedom to choose the numbering of the sites within each triangle, and that the convention of Fig. 1 is different from that of Ref. 27.

With a little algebra, we write the effective Hamiltonian in a more compact way. Indeed, the operators τ_i^+ and τ_i^- can be rewritten by introducing τ_i^x and τ_i^y :

$$\begin{aligned}\tau_i^+ &= \tau_i^x + i\tau_i^y, \\ \tau_i^- &= \tau_i^x - i\tau_i^y.\end{aligned}$$

Hence, $\alpha_{ij}\tau_i^- + \alpha_{ij}^2\tau_i^+ = (\alpha_{ij} + \alpha_{ij}^2)\tau_i^x + i(\alpha_{ij}^2 - \alpha_{ij})\tau_i^y$, and therefore:

$$\alpha_{ij}\tau_i^- + \alpha_{ij}^2\tau_i^+ = \begin{cases} 2\tau_i^x & \text{if } \alpha_{ij} = 1 \\ -\tau_i^x - \sqrt{3}\tau_i^y & \text{if } \alpha_{ij} = \omega^2 \\ -\tau_i^x + \sqrt{3}\tau_i^y & \text{if } \alpha_{ij} = \omega. \end{cases}$$

The notation is further simplified by introducing three unitary vectors $\vec{e}_1 = (1,0)$, $\vec{e}_2 = (-\frac{1}{2}, -\frac{\sqrt{3}}{2})$, $\vec{e}_3 = (-\frac{1}{2}, \frac{\sqrt{3}}{2})$:

$$\alpha_{ij}\tau_i^- + \alpha_{ij}^2\tau_i^+ = \begin{cases} 2\vec{\tau}_i \cdot \vec{e}_1 & \text{if } \alpha_{ij} = 1 \\ 2\vec{\tau}_i \cdot \vec{e}_2 & \text{if } \alpha_{ij} = \omega^2 \\ 2\vec{\tau}_i \cdot \vec{e}_3 & \text{if } \alpha_{ij} = \omega. \end{cases}$$

With this notation, the Hamiltonian reads:

$$\mathcal{H}_0^{\text{eff}} = \frac{J'}{9} \sum'_{\langle i,j \rangle} \vec{\sigma}_i \cdot \vec{\sigma}_j (1 - 4\vec{e}_{ij} \cdot \vec{\tau}_i)(1 - 4\vec{e}_{ij} \cdot \vec{\tau}_j), \quad (2)$$

where the vectors \vec{e}_{ij} are to be chosen among \vec{e}_1 , \vec{e}_2 , and \vec{e}_3 . In this Hamiltonian, we treat $\vec{\sigma}_i$ and $\vec{\tau}_i$ as classical vectors with norm 1 and 1/2, respectively. By adopting the gauge depicted in Fig. 1, we end up with a triangular lattice having each bond characterized by a vector \vec{e}_μ , with $\mu = 1, 2, 3$. In Fig. 2, the different lines indicate which \vec{e}_μ has to be taken for \vec{e}_{ij} in the effective Hamiltonian.

Hereafter, we consider the classical limit of the effective Hamiltonian and we prefer to normalize both spin and chirality to unity, which leads to

$$\mathcal{H}_0^{\text{eff}} = \frac{J'}{9} \sum'_{\langle i,j \rangle} \vec{\sigma}_i \cdot \vec{\sigma}_j (1 - 2\vec{e}_{ij} \cdot \vec{\tau}_i)(1 - 2\vec{e}_{ij} \cdot \vec{\tau}_j). \quad (3)$$

In this Hamiltonian, the presence of the chiralities has the effect of changing the coupling between spins. We will see that this leads to a complicated interplay between spins and chiralities and gives rise to a very rich physics in the low-temperature regime.

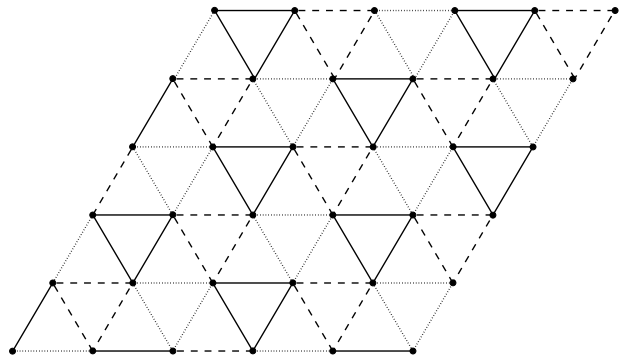


FIG. 2: Triangular lattice on which the effective Hamiltonian is defined. The unitary vector for the bond is indicated by solid lines ($\vec{e}_\mu = \vec{e}_1$), dashed lines ($\vec{e}_\mu = \vec{e}_2$), and dotted lines ($\vec{e}_\mu = \vec{e}_3$).

III. ZERO-FIELD PROPERTIES

In this section we present the results of our model when no external magnetic field is applied. We provide evidences that, for low-enough temperatures, the system undergoes a partial *order by disorder* transition to a state where the chiralities are essentially frozen in a given configuration.

A. Ground state manifold

In order to investigate the interplay between spins and chiralities, let us first study the low-temperature properties of the system. This is achieved by performing classical Monte Carlo simulations using a heat-bath algorithm.³⁰ In the context of our model, the heat-bath algorithm is efficient down to very low temperatures ($T/J' \approx 10^{-6}$), and, therefore, it is possible to have insight into very low-energy phases. The details of this algorithm are discussed in Appendix A. For most calculations, we considered an 18×18 triangular lattice with periodic boundary conditions, and we checked the conclusions on larger sizes. However, as we will show in the following, for all temperatures, the physical properties are governed by short-range correlations and, therefore, the 18×18 lattice is enough to obtain insight into the thermodynamic limit.

The first important outcome is that the energy per site converges to $\epsilon = -J'/2$ when $T \rightarrow 0$. The particularly simple value of the ground state energy deserves some further investigation. If we look back at the Hamiltonian defined by Eq. (3), we can find several classes of states that have energy $\epsilon = -J'/2$. For instance, when all the chiralities are parallel to a given vector $\vec{\gamma}$ in the XY plane defined by the vectors \vec{e}_μ , then the two factors involving the chiralities in Eq. (3) become equal, leading to a non-negative coupling between the spins, and the energy is minimized by a 120° Néel state for the spin

vectors. Then, the energy for an N -site system becomes:

$$E = -\frac{J'}{18}N \sum_{\mu=1,2,3} (1 - 2\vec{\gamma} \cdot \vec{e}_\mu)^2 = -\frac{J'}{2}N, \quad (4)$$

independently of the direction $\vec{\gamma}$ of the chiralities in the XY plane. Therefore, we obtain a large class of states which have, beside the usual rotational symmetry of the Néel state of the spins $\vec{\sigma}$, an extra continuous symmetry in $\vec{\tau}$ space.

Another important class of states is defined by those configurations that have chiralities anti-parallel to the vectors \vec{e}_μ , independently on each site. In this case, the coupling of one site to four out of its six neighbors vanishes. Indeed, we have that \vec{e}_μ is equal to \vec{e}_1 for the bond with two neighbors, \vec{e}_2 with two other neighbors and \vec{e}_3 for the last two bonds (see Fig. 2). For any choice of $\vec{\tau}_k$ among the three possible $-\vec{e}_\mu$, the effective magnetic coupling vanishes for the four bonds where $\vec{\tau}_k \cdot \vec{e}_{kj} = \frac{1}{2}$ since it contains the factor $(1 - 2\vec{e}_{kj} \cdot \vec{\tau}_k)(1 - 2\vec{e}_{kj} \cdot \vec{\tau}_j)$. Moreover, having taken $\vec{\tau}_k = -\vec{e}_\nu$, the effective magnetic coupling with the remaining two neighbors is non-zero only if $\vec{\tau}_j$ is equal to $-\vec{e}_\nu = \vec{\tau}_k$. In this case, the effective interaction between the two sites is equal to J' .

A given site k can therefore interact with its neighbors in three different ways. It might be coupled to two neighbors, l and m , in which case these two neighbors will also be coupled, because they have parallel chiralities and $\vec{e}_{lm} = \vec{e}_{kl} = \vec{e}_{km}$. In that way, we create a coupled triangle, which is completely disconnected from the rest of the lattice. The site k might also be coupled to one neighbor only, forming a system of two coupled spins. The third possibility is to have the site completely disconnected from its neighbors. A typical coupling pattern is shown in Fig. 3. Hereafter, we denote by dimer the system of two coupled spins. It is worth mentioning that because of the classical nature of the spins, the dimer is a classical object, with gapless excitations, and it has nothing to do with the quantum dimers, which are gapped objects.

When the chiralities are opposite to the \vec{e}_μ , the coupling pattern will only exhibit isolated sites, dimers and triangles. Moreover, any of these patterns that one can draw on the triangular lattice can also be achieved by choosing the appropriate chiralities. Having fixed the chiralities, the energy is minimized with opposite spins on the dimers and the energy per spin is $\epsilon = -J'/2$; on an isolated triangle, the sum of the spins needs to be zero, the energy per spin being again $\epsilon = -J'/2$; finally isolated sites do not contribute to the energy. Hence, among the possible configurations of chiralities opposite to \vec{e}_μ , those that do not have isolated spins have the ground state energy per site $\epsilon = -J'/2$.

A direct inspection of the chiralities and spins in our Monte Carlo simulations shows that when the system is cooled down abruptly from infinite temperature, that is by starting at the chosen temperature from a random configuration for the spins and the chiralities, states with

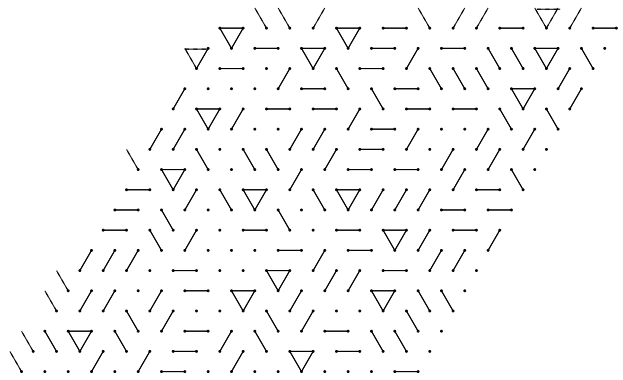


FIG. 3: Generic coupling pattern for random chiralities opposite to the vectors \vec{e}_μ . Notice that, because of the periodic boundary conditions, some of the bonds (indicated by dashed lines) connect sites on opposite sides of the lattice.

no obvious pattern in the chiralities and energy per site $\epsilon = -J'/2$ are achieved. Therefore, the two particular classes of states described above are only two among many other ground states. On the contrary, by cooling down the system through a finite number of temperatures and letting it thermalize at every step before cooling down to the next nearby temperature, we obtain a configuration with disconnected triangles and dimers. Within the heat-bath Monte Carlo, this fact strongly indicates the presence of a partial *order by disorder* effect: Among all the possible ground states, the states with large entropy are selected by thermal fluctuations. In the following, we will describe in more details the entropic selection that appears at low-enough temperature, describing how this transition affects the spin dynamics.

B. Entropic selection of a family of ground states

At temperature $T/J' = 10^{-6}$, the Monte Carlo results show that the chiralities are frozen on each site in the XY plane opposite to the \vec{e}_μ vectors in such a way as to create a collection of disconnected dimers and triangles. The selection of this specific class of states can be explained by its large entropy. Within each decoupled triangle and dimer, the spins are totally free to rotate as long as their sum vanishes *independently* of the spins of the other triangles and dimers. Thus, all those states have a huge entropy at low-enough temperature. It can easily be proved that both for dimers and triangles, every site carries one degree of freedom that does not change the energy. This point is discussed in more details below in the section devoted to the specific heat. As the system is cooled down slowly, these states with largest entropy are selected. The ground state degeneracy is partially lifted by thermal fluctuations and an entropic *order by disorder* effect is observed.

In Fig. 4, we show how the non-zero couplings are typically distributed over the lattice at $T/J' = 10^{-6}$. We do

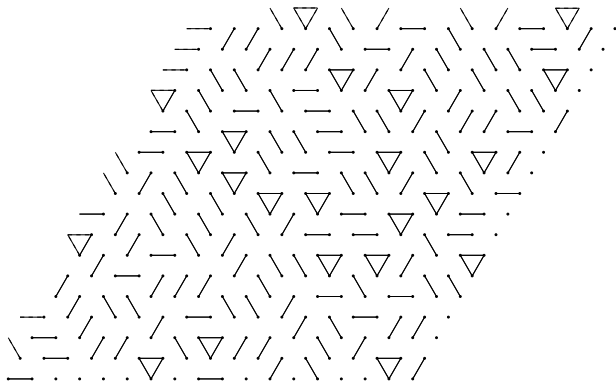


FIG. 4: Typical coupling pattern at $T/J' = 10^{-6}$: The solid lines between the sites indicate a non-zero coupling between the spins. Notice that, because of the periodic boundary conditions, some of the bonds (indicated by dashed lines) connect sites on opposite sides of the lattice.

not have any evidence that the system prefers to create triangles or dimers: We have performed several simulations starting from different random orientations, and in all cases we have reached a state which contains both triangles and dimers. The average number of triangles is 17 on an 18×18 site cluster, and the distribution is peaked around this number with a mean square displacement of 3. We suspect that this simply corresponds to the distribution for all coverings of the triangular lattice by triangles and dimers. In any case, this observation agrees with the fact that, at low temperature, triangles and dimers have the same entropy per site.

To have more insight into this entropic selection, we report the chiralities in the XY plane for decreasing temperatures in Fig. 5. As the system is cooled down below $T^* \approx 0.05J'$, the chiralities start to display a short-range order in the XY plane, getting more and more anti-parallel to the \vec{e}_μ vectors. As far as we can tell, this cross-over temperature does not depend on the cooling rate, provided it is not too fast. The results reported in Fig. 5 have been obtained after performing 10^4 sweeps over the lattice at each intermediate temperature starting from a random configuration, but the same behaviors have been observed with different numbers of sweeps.

Since the chirality configurations that can be selected by the *order by disorder* mechanism form an infinite but *discrete* set, one can expect that, once such a state has been reached, the system will somehow be trapped in this state. This is indeed the case on short time scales. However, whether this corresponds to a true freezing transition requires a careful study of the low temperature dynamics. For instance, in 2D models of spin glasses with short range interactions, the actual freezing on arbitrarily large time scales only takes place at zero temperature. So we now turn to a careful analysis of the low-temperature spin and chirality dynamics.

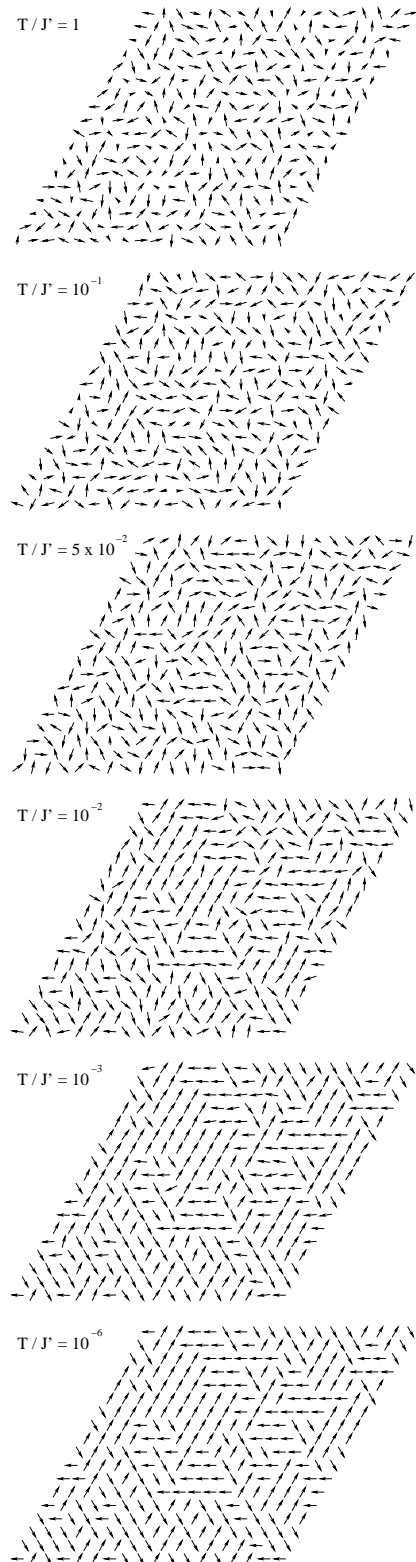


FIG. 5: Configuration of the chiralities in the XY plane for different temperatures.

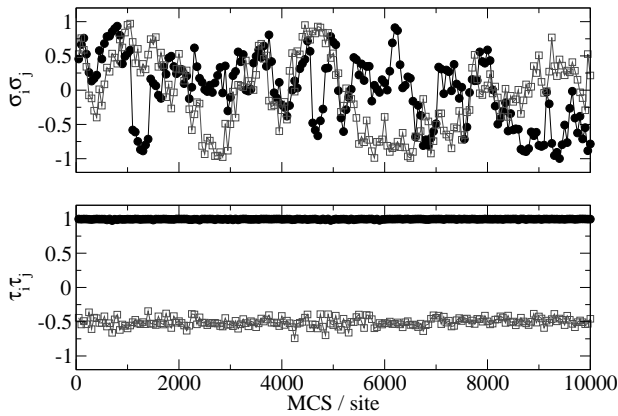


FIG. 6: Spin-spin (upper panel) and chirality-chirality (lower panel) correlations at $T/J' = 10^{-3}$ for two non-nearest-neighbor sites with parallel (full symbols) and non-parallel (open symbols) chiralities.

C. Low-temperature spin and chirality dynamics

Below T^* , spins and chiralities behave very differently. Whereas the chiralities are frozen on short time scales, spins are expected to continue to have a fast dynamics since, once the lattice is decoupled into disconnected dimers and triangles, the spins belonging to each of these elementary building blocks are free to rotate as long as the total spin of the dimer or of the triangle remains zero. Spin-spin and chirality-chirality correlation functions confirm this fact. In Fig. 6, we show typical non-nearest-neighbor correlations $\vec{\sigma}_i(t) \cdot \vec{\sigma}_j(t)$ and $\vec{\tau}_i(t) \cdot \vec{\tau}_j(t)$ as a function of the time after the system has reached equilibrium at $T/J' = 10^{-3}$. Throughout, the time unit is one Monte Carlo sweep over the entire lattice. Indeed, the spin-spin correlation function for non-nearest-neighbors fluctuates wildly on short time scales, while the chirality-chirality correlation function is essentially constant. By contrast, the spin-spin correlations for a pair of coupled nearest-neighbor sites are fixed to -1 or $-1/2$ for dimers or triangles, respectively (not shown).

On short time scales, the chiralities are frozen below T^* and although there is a huge class of energetically and entropically equivalent states, once one configuration is achieved, the system cannot switch to another one. The different configurations must therefore be separated by large energy barriers and the chiralities remain trapped in a small region of their phase space. A similar behavior is observed in ordinary spin-glass materials, where the spin degrees of freedom are completely frozen below a given temperature and different states are separated by infinite (in the thermodynamic limit) energy barriers. In this case, the transition temperature can be characterized by the divergence of the spin-glass susceptibility

$$\chi_{\text{SG}}^\sigma = \frac{1}{N} \sum_{i,j} \left[\frac{1}{t_{\text{exp}}} \sum_{t=1}^{t_{\text{exp}}} \vec{\sigma}_i(t) \cdot \vec{\sigma}_j(t) \right]^2, \quad (5)$$

where the average over the time (Monte Carlo steps) is done over a sufficiently large period t_{exp} , corresponding to the time scale of the experiment. In ordinary spin glasses, χ_{SG}^σ is zero (very small on finite systems) for temperatures above the critical temperature, where the spins have a fast dynamics, and becomes finite below the critical temperature, indicating that the spins are frozen in a given configuration. In particular, at low temperature, χ_{SG}^σ grows linearly with the number of sites N .

By analogy, in our model, we can define a spin-glass susceptibility for the chirality pseudo-spins:

$$\chi_{\text{SG}}^\tau = \frac{1}{N} \sum_{i,j} \left[\frac{1}{t_{\text{exp}}} \sum_{t=1}^{t_{\text{exp}}} \vec{\tau}_i(t) \cdot \vec{\tau}_j(t) \right]^2, \quad (6)$$

and try to identify a transition temperature from the high-temperature disordered phase to the low-temperature frozen phase. It turns out that, like in 2D disordered spin models, the freezing takes place at finite temperatures only for finite time scales, and that the actual phase transition, if any, presumably takes place at zero temperature. To see this, we have plotted in Fig. 7 the chirality susceptibility χ_{SG}^τ as a function of temperature for different *experimental* times t_{exp} , corresponding in this case, to the time we have waited at each temperature during the cooling process. For a given time scale, one can clearly identify two regimes: At high temperatures χ_{SG}^τ/N is very small, due to the dynamical character of the chirality variables, whereas for T/J' small enough, there is a clear enhancement of χ_{SG}^τ/N , indicating a frozen dynamics of the chiralities. However, the temperature at which this change of behavior takes place depends on the time of the simulation. To quantify this dependence, we have plotted the freezing temperature T_f at which the susceptibility reaches half the value it will take at zero temperature as a function of t_{exp} . Clearly T_f decreases with t_{exp} , and for times $t_{\text{exp}} > 10^5$, the two are related by $t_{\text{exp}} = t_0 \exp(E_0/T_f)$, or equivalently $T_f = E_0 / \log(t_{\text{exp}}/t_0)$, with $E_0 \simeq 0.07J'$ and $t_0 \simeq 6500$.

This fit shows that, at any temperature, the chirality configuration will change on large enough time scales, and that the process is thermally activated with an activation energy E_0 . This energy can thus be interpreted as the typical free-energy barrier between two configurations selected by the *order by disorder* mechanism. As in the model of Ref.28, the freezing temperature T_f has only a weak logarithmic dependence on the time scale.

Note that these results are not affected by the size (18×18) used in the simulation. Indeed we have checked in a number of cases that the conclusions are qualitatively and quantitatively similar for 27×27 and 36×36 clusters. In particular, for a given t_{exp} , the temperature T_f does not change upon increasing the size of the cluster.

To summarize, we found that spins and chiralities have very different low temperature dynamics in zero field. At a cross-over temperature $T^* \simeq 0.05J'$, chirality configurations with maximum entropy are selected. Below this temperature, the chirality dynamics is activated with a

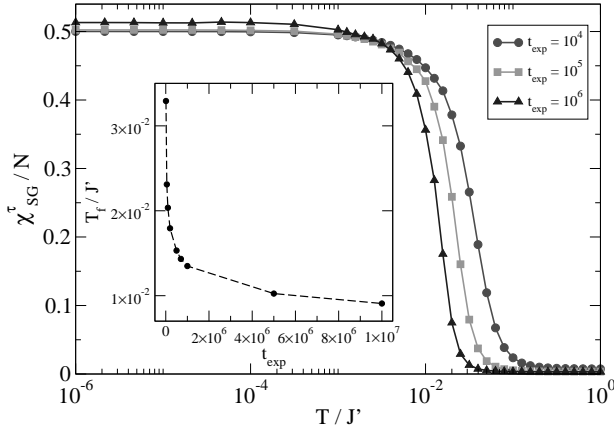


FIG. 7: Chiral spin-glass susceptibility per site χ_{SG}^{τ}/N as a function of the temperature for different time scales t_{exp} . Inset: Variation of the freezing temperature T_f with t_{exp} . Lines are guides to the eye.

an energy barrier $E_0 \simeq 0.07J'$ and it is already extremely slow at $T = 0.01J'$, while the spins retain a very fast dynamics down to the lowest temperatures. The spins do not behave as free spins however, as we shall see in the following section, and the freezing of the chiralities has important consequences on the response of the spins in the presence of an external magnetic field.

D. Specific heat

On very general grounds, we can expect that the cross-over from the high-temperature disordered phase to the low-temperature phase where chirality configurations have been selected by the *order by disorder* mechanism is marked by a peak in the specific heat. Whereas for a true phase transition the specific heat diverges at the critical temperature, for freezing phase transitions, like in spin-glass systems, the specific heat exhibits a rather broad peak near the freezing temperature.²⁵ This is indeed what we observe in our model. We calculate the specific heat using $C_V = (\langle E^2 \rangle - \langle E \rangle^2)/T^2$, where $E = E(T)$ is the internal energy. The specific heat per spin shows a broad peak which does not increase with the size of the lattice for $T \simeq T^* \simeq 0,05J'$ (see Fig. 8).

The low-temperature value of the specific heat, namely $3/2$ per site, is a very nice confirmation of the picture. For classical variables, each quadratic mode gives a contribution to the specific heat equal to $1/2$ in units of k_B . Thus, if both spin and chirality were ordered at low temperature, we would expect the zero temperature specific heat per site to be equal to 2. According to our picture however, only the chiralities are ordered. In a given configuration that minimizes the entropy, each chirality can fluctuate around its reference direction $-\vec{e}_{\mu}$ with two quadratic modes corresponding to two orthogonal directions, and its contribution to the specific heat is equal to

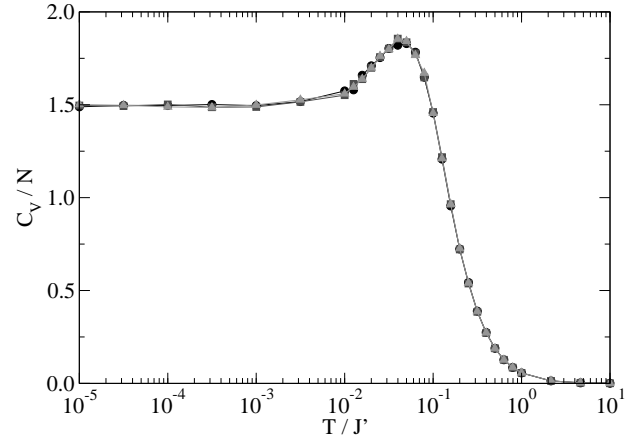


FIG. 8: Specific heat C_V per spin as a function of the temperature for different lattices: 18×18 (circles), 27×27 (squares), and 36×36 (triangles). Lines are guides to the eye.

1. However, within a triangle or a dimer, the spins are free to rotate as long as their sum is equal to zero. This means that they have zero-energy modes which do not contribute to the specific heat. For a dimer, the common direction of the vectors can rotate freely, while the relative direction gives rise to two quadratic modes, so one effectively gets one quadratic mode per spin. In a triangle, if we consider a configuration where the sum of the spins is equal to zero, the orientation of a given spin is arbitrary, which gives rise to two zero-energy modes, and the others are free to rotate around the direction of the first one, which gives a third zero-energy mode. So we are left with 3 quadratic modes, i.e. one quadratic mode per spin, like in a dimer. So the spin contribution to the specific heat is $1/2$ per site, and the total specific heat per site is equal to $3/2$. Note that the entropy is thus the same for triangles and dimers, as stated above.

The reduction of the spin contribution to the specific heat by a factor 2 is quite remarkable. This should be compared for instance with the classical Heisenberg model on the *kagome* lattice, in which case the zero temperature specific heat is reduced from 1 to $11/12$ (see Ref.14).

IV. FINITE-FIELD PROPERTIES

In the absence of an external magnetic field the chiralities show a behavior reminiscent of spin glasses. In ordinary spin-glass materials, the freezing of the degrees of freedom, together with a complicated energy landscape, has consequences on the magnetic properties of the system. Even though in our model the spins retain a fast dynamics even below T^* , the freezing of the chiralities might still induce non-trivial properties when an external magnetic field is present. In the following, we consider an external magnetic field that is coupled to the spins

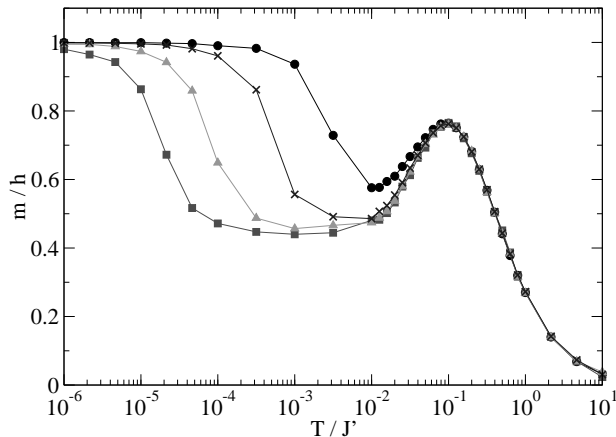


FIG. 9: The equilibrium magnetization per spin in units of h as a function of the temperature, for $h/J' = 10^{-2}$ (squares), 2×10^{-2} (triangles), 5×10^{-2} (crosses), 10^{-1} (circles). Lines are guides to the eye.

and we study the dynamical response of the spins.

A. Equilibrium magnetization

The Hamiltonian in the presence of an external magnetic field h along the z axis reads:

$$\mathcal{H}^{\text{eff}} = \mathcal{H}_0^{\text{eff}} + h \sum_i \sigma_i^z. \quad (7)$$

First, we concentrate on the equilibrium magnetization of the system as a function of the temperature. In order to find the equilibrium magnetization per site m , we perform a very long simulation, cooling down the system through a finite number of intermediate temperatures in the presence of the external magnetic field. At each temperature, we equilibrate the system, by considering a large number of Monte Carlo steps: This kind of protocol is known as a *field-cooled* (FC) experiment. Within this procedure, we are able to obtain accurate results for the equilibrium curve for the magnetization as a function of the temperature.

In Fig. 9, we report the results for the magnetization per site as a function of the temperature, for different values of the external magnetic field h . We can distinguish three different regimes. In the first one, common to all the cases and corresponding to $T/J' \gtrsim 0.1$, the chiralities are randomly distributed and are free to rotate, retaining a quite fast dynamics. Therefore, $\langle \vec{e}_{ij} \cdot \vec{\tau}_j \rangle \approx 0$, implying that the effective Hamiltonian reduces to a Heisenberg model on a triangular lattice, with an effective antiferromagnetic coupling $J^{\text{eff}} \approx J'/9$ [see Eq. (3)].

In the second regime, whose temperature range strongly depends on the value of the magnetic field, the magnetization decreases and shows a plateau whose width depends on the actual value of the external mag-

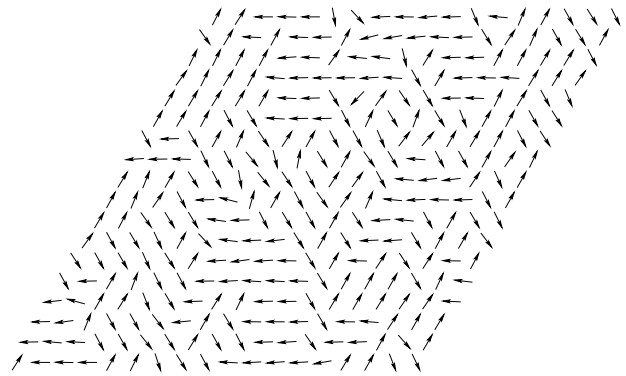


FIG. 10: Configuration of the chiralities in the XY plane for $T/J' = 10^{-6}$ and an external magnetic field $h/J' = 10^{-2}$.

netic field. This behavior can be explained by the establishment of a short-range order of the chiralities, which become opposite to the vectors \vec{e}_μ , like in the $h = 0$ case. In this regime, the free energy is minimized because of the high entropy of the spins, the physical properties are mostly determined by disconnected dimers and triangles and the actual value of the magnetization depends on the number of dimers and triangles, being $m = h/(2J')$ for the former case and $m = h/(3J')$ for the latter case.

By further lowering the temperature, the entropic part of the free energy becomes less important and the chiralities rearrange by slightly modifying their ordering, allowing the spins to increase their magnetization as the system reaches its actual ground state for finite h . As $T \rightarrow 0$, the magnetization per site goes to $m_{\text{max}} = h/J'$. A direct inspection of the chiralities, see Fig. 10, shows that their low-temperature configuration is only slightly modified from the $h = 0$ case. However, this is sufficient to change considerably the magnetization. The low temperature $T_m(h)$ at which the magnetization finally increases indicates that there is a very small energy difference between the actual ground state and the states described by dimers and triangles.

As shown in Fig. 9, the qualitative behavior of the equilibrium magnetization is the same for different values of h . However, as the external field gets bigger, the magnetization starts increasing towards its saturation value for higher temperatures. Therefore, $T_m(h)$ strongly depends upon the external magnetic field and increases with h . On the contrary, the formation of dimers and triangles, determined by the maximum of the magnetization at $T/J' \sim 0.1$, does not depend on the external magnetic field, indicating that T^* does not change with the application of h . The important fact is that, at a given temperature below T^* , the magnetization is no longer a linear function of the applied external field, as typical magnetization curves show in Fig. 11.

For small magnetic fields, the system is in the regime with disconnected dimers and triangle, which have a linear magnetization $m = h/(2J')$ and $m = h/(3J')$, respectively. Therefore, the total magnetization is also linear in

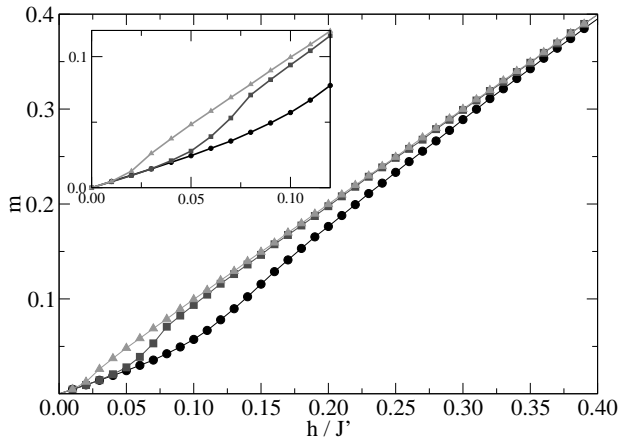


FIG. 11: Magnetization per site as a function of the external field at $T/J' = 10^{-4}$ (triangles), $T/J' = 10^{-3}$ (squares) and $T/J' = 10^{-2}$ (circles). The lines are guides to the eye.

h with a coefficient that depends on the actual number of triangles and dimers. For larger h , the magnetization goes through a highly non-linear region, characterized by a complicated interplay between spins and chiralities. In this regime, the entropy is maximized with chiralities opposite to the vectors \vec{e}_μ , whereas the energy is minimized with configurations that lead to a bigger magnetization. Eventually, the chiralities order in such a way as to allow the spins to have a magnetization $m = h/J'$ and the system is again in a linear regime. A consequence of this competition between different states is visible in the dynamical properties of the system.

B. Dynamical magnetization and slow spin dynamics

In order to investigate the interplay between spins and chiralities and its effect on the dynamical properties of the system, we perform a *zero-field cooled* (ZFC) numerical experiment: The system is slowly cooled down to the temperature of interest in the absence of an external magnetic field. Then, an external magnetic field is turned on and we observe the magnetization as a function of time. Fig. 12 shows the result for three different external fields $h/J' = 0.02$, $h/J' = 0.07$ and $h/J' = 0.15$ at $T/J' = 10^{-3}$. At equilibrium, the first field will bring the system into a regime with disconnected dimers and triangles and magnetization $h/(3J') \leq m \leq h/(2J')$ (corresponding to the plateau region of Fig. 9). The third field will generate a state with chiralities slightly different from the opposite vectors \vec{e}_μ and magnetization $m \sim h/J'$ (corresponding to the bump of Fig. 9 at very low temperatures), whereas the second field represents the intermediate regime.

For $h/J' = 0.02$ we observe that the system acquires its final magnetization in a very small number of Monte

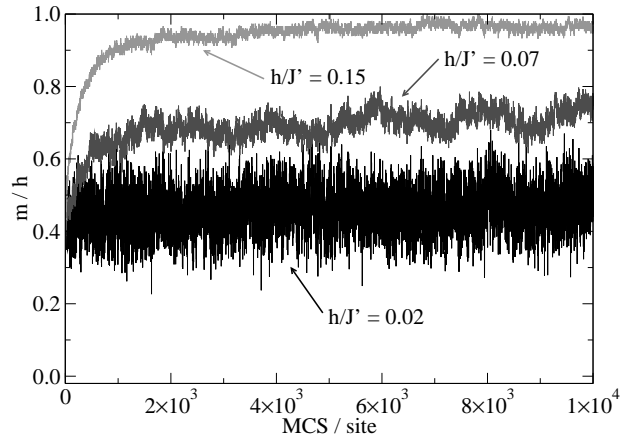


FIG. 12: Magnetization per site in units of the external field as a function of the Monte Carlo steps for $h/J' = 0.02$, $h/J' = 0.07$ and $h/J' = 0.15$. The temperature is $T/J' = 10^{-3}$.

Carlo steps, through a very fast process, typical of non-frustrated systems. This can be understood because, just before turning on the magnetic field, the system already displays a collection of dimers and triangles. When the external field is turned on, the spins quickly arrange to minimize the energy. In this process, the chiralities do not change from their previous equilibrium position. On the contrary, when a field $h/J' = 0.07$ or $h/J' = 0.15$ is switched on, the final equilibrium magnetization is reached only after a much longer simulation time. As in the previous case, the system very quickly acquires a magnetization corresponding to the magnetization of a system of triangles and dimers. However, after this first very rapid process, a much slower dynamics takes place, during which the chiralities and spins find a compromise to minimize the free energy. Indeed, as soon as the chiralities start to couple the triangles and dimers with their neighbors, the spins are no longer free to move independently and they start to have a slower dynamics. In this case the magnetization obtained after a short time is different from the equilibrium magnetization.

A further confirmation of the very slow spin response to a magnetic field is given by the difference between the magnetization curve as a function of the time for the FC and the ZFC protocols, see Fig. 13. In the following, we concentrate on the case $T/J' = 10^{-6}$ and $h/J' = 10^{-2}$. Let us first consider the ZFC magnetization. As long as $h = 0$, the magnetization vanishes and the chiralities are all opposite to the vectors \vec{e}_μ and there are both triangles and dimers in the coupling pattern. When the external magnetic field is turned on, the magnetization reaches the value $m \approx 0.004$ in about 20 Monte Carlo steps. This first very rapid regime corresponds to the spins moving toward the direction of the magnetic field. During this fast spin dynamics, the chirality does not play any important role in the dynamical process. Indeed, we have verified that $m \sim 0.004$ is also the magnetization acquired in the first 20 Monte Carlo steps within a simulations where

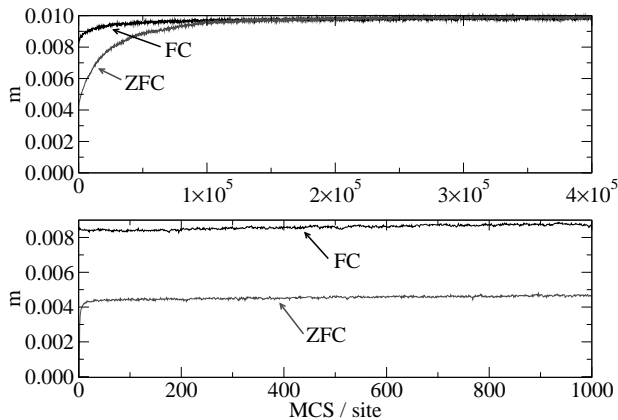


FIG. 13: Long-time (upper panel) and short-time (lower panel) behavior of the magnetization per spin versus time at $T/J' = 10^{-6}$ for a FC and a ZFC protocol. The external field has magnitude $h/J' = 10^{-2}$.

the chiralities were kept fixed. In the second regime, the magnetization increases very slowly up to its saturation value $m \sim h/J'$. This slow increase is due to the combined dynamics of spins and chiralities, in order to find a compromise to minimize the free energy. By contrast, within the FC protocol, the system is cooled down in the presence of the external magnetic field and therefore, at the final temperature, the magnetization has already a finite value $m \sim 0.0085$ and the chiralities are no longer in the direction of the basis vectors. Then, by keeping the system at the desired temperature $T < T_m(h)$, a very slow increase of the magnetization is observed, similar to the behavior of the second regime of ZFC.

The pronounced difference between the ZFC and the FC protocols, and more generally an evident *aging* effect has already been emphasized in a related, but much simpler classical model containing two different Ising variables.²⁸ Finding the same kind of behavior in a more realistic Hamiltonian demonstrates that this is a robust feature of models with competing variables and frustrating interactions, even in the absence of an explicit disorder like in ordinary spin-glass materials.

V. CONCLUSIONS

In this paper we have investigated the properties of the classical version of an effective Hamiltonian for the $S = 1/2$ Heisenberg antiferromagnet on a *trimerized kagome* lattice using classical Monte Carlo methods. The analysis of this model shows many interesting features, possibly reminiscent of a spin-glass behavior at low temperatures. The fully frustrated character of the interaction, due to the presence of two kinds of variables on each site, induces a freezing of the chiralities and, in the presence of an external magnetic field, the development of very large time scales for the spins at low temperature.

Indeed, we have demonstrated that, by a partial *order by disorder* effect, for $T \lesssim T^* \approx 0.05J'$, the states with highest entropy are selected by thermal fluctuations, and the chiralities freeze along particular directions. This prevents the system from developing any long-range correlations and completely splits the lattice into disconnected dimers and triangles, with antiferromagnetically coupled spins. On each of these elementary entities the spins are free to rotate, as long as they add up to zero.

When the spins are coupled to an external magnetic field and the temperature is sufficiently small, the freezing of the chiralities has a strong effect on the low-temperature spin properties. First of all, the equilibrium magnetization for small magnetic fields has a clear non-linear behavior, whereas for large enough h , we obtain $m \propto h$. The actual magnetic field range for which the non-linear behavior is detected strongly depends upon the temperature. However, the non-linearity cannot be meaningfully casted into a divergent χ_3 , in contrast to traditional spin glasses. Still, very strong non-linear effects in the magnetization curves are clearly present and point to a spin-glass reminiscent behavior. Secondly, there is a clear difference between the FC and the ZFC measurements of the magnetization, typical of spin-glass models. A difference with ordinary spin-glass systems, representing an original aspect of our results is that the characteristic temperature T_m below which the slow spin response takes place does not coincide with T^* and strongly depends on the external magnetic field, i.e., $T_m = T_m(h)$. On the other hand, the freezing transition of an ordinary spin glass corresponds to a thermodynamic transition and the freezing temperature is independent of the particular protocol. Nonetheless, the very slow spin response to an external magnetic field is typical of ordinary out-of-equilibrium systems, and here it is driven by the freezing of the chiralities. In this respect, the richness of our model consists in having two distinct temperatures, i.e., T^* , which characterizes the entropic selection of chirality configurations, and $T_m(h)$, which characterizes the establishment of the slow spin dynamics. On the contrary, in the ordinary spin-glass models, there is only one characteristic temperature.

So the results we have obtained on the classical version of the effective model of the $S=1/2$ Heisenberg model on the trimerized *kagome* clearly show that the interplay of two local degrees of freedom can lead to a very slow dynamics, and to a behavior which is in many respects reminiscent of the spin-glass phenomenology. One point worth noticing at that stage is that this behavior is, as far as we can tell, independent of the dynamics chosen in the numerical simulations. In particular, we have performed a few simulations with simultaneous updates of spins and chiralities at the same site, and the results were unchanged. This is a clear improvement over the simplified model of Ref. 28, in which the entropic barriers were related to the dynamics. The present results suggest that the development of a very slow dynamics is actually a generic feature of models with two local de-

degrees of freedom.

Coming back to the experimental evidence in favor of a spin-glass behavior in $\text{SrCr}_{8-x}\text{Ga}_{4+x}\text{O}_{19}$, the present results are very promising in several respects. First of all, the model was motivated by physical considerations of the exchange processes in this system, in which the *kagome* layers are trimerized. Besides, the broken ergodicity which is at the origin of the very slow dynamics is neither related to a specific dynamics nor to disorder but to the presence of two local degrees of freedom, a very natural consequence of the special topology of the trimerized *kagome* lattice. In particular, although we started from spins 1/2, all half-integer spin models on the trimerized *kagome* lattice lead to very similar effective models with two local degrees of freedom.²⁹ In addition, the characteristic temperature at which large time scales appear is much lower than the coupling constant, again in agreement with $\text{SrCr}_{8-x}\text{Ga}_{4+x}\text{O}_{19}$. Finally, the spins have a very anomalous response to magnetic field, with a clear difference between field-cooled and zero-field-cooled protocols, while retaining a very fast dynamics at low temperatures. As far as we know, this is a unique feature of the present model, which could be related to the muon spin rotation observation that only a tiny part of the spins are actually frozen in $\text{SrCr}_{8-x}\text{Ga}_{4+x}\text{O}_{19}$ below the spin-glass transition.³¹

There are clear differences however between our model and the properties of $\text{SrCr}_{8-x}\text{Ga}_{4+x}\text{O}_{19}$. An obvious one is the specific heat, which is quadratic below the spin-glass transition, whereas in our model it goes to a constant. This behavior is clearly a consequence of our approximation to treat spin and chirality degrees of freedom as classical variables. Given the quasi-two dimensionality of the compound, one can speculate that a quantum treatment would lead to a T^2 behavior of the specific heat for the quadratic degrees of freedom, in agreement with experiments. This could actually be a natural explanation of this behavior, which is *not* the most common behavior in spin glasses, which tend to have a linear specific heat at low temperature. At that stage, the main discrepancy between the phenomenology described in the present paper and the experimental results obtained in $\text{SrCr}_{8-x}\text{Ga}_{4+x}\text{O}_{19}$ is the observation of a clear phase transition in this compound with a divergent non-linear susceptibility. It is likely that a true phase transition would require to include inter-layer coupling, like in disordered models of spin-glasses. Whether including such a coupling can produce a divergent non-linear susceptibility is left for future investigation. We should also note that the effective model for spins 1/2 has specific features with respect to the effective models for larger half-integer spins. In particular, the identification of exact ground states does not seem to be possible for larger spins,²⁹ and the phenomenology of these models might turn out to be different in some respects, although we are confident that the presence of two degrees of freedom will still lead to an anomalous response of the spins to an external magnetic field and to the development of large

time scales.

Acknowledgments

It is a pleasure to thank J.-P. Bouchaud, D. Dean, P. Delos Rios, S. Franz, M. Mambrini, M. Sellitto, F. Ricci Tersenghi, and M. Zhitomirsky for enlightening discussions. This work has been supported by the Swiss National Fund and by Istituto Nazionale per la Fisica della Materia (INFN).

APPENDIX A: MONTE CARLO TECHNIQUE

In this Appendix, we describe the Monte Carlo method used throughout our study. For simplicity, let us consider the Hamiltonian:

$$\mathcal{H} = \sum_{\langle i,j \rangle} J_{ij} \vec{\sigma}_i \cdot \vec{\sigma}_j, \quad (\text{A1})$$

where $\vec{\sigma}_i$ are classical unit spin vectors on the sites of an N -site lattice and J_{ij} are magnetic couplings.

In order to study the dynamics of this Hamiltonian, we have performed Monte Carlo simulations using the heat-bath algorithm to update the vector directions.³⁰ Each spin is assumed to be in contact with a heat bath and is immediately put into a local equilibrium with respect to the instantaneous effective field on it from the nearest neighbor spins:

$$\vec{H}_i = \frac{1}{T} \sum_{\langle j \rangle_i} J_{ij} \vec{\sigma}_j, \quad (\text{A2})$$

where $\langle j \rangle_i$ indicates the nearest neighbors of the site i and T is the temperature.

The new direction of a given spin is determined by a polar angle θ and an azimuthal angle ϕ relative to \vec{H}_i , through the following Boltzmann distribution:

$$P(\cos \theta) = \frac{H}{2 \sinh H} e^{H \cos \theta}, \quad (\text{A3})$$

where $H = |\vec{H}_i|$. The two angles θ and ϕ are chosen with the use of two random numbers R_1 and R_2 , uniformly distributed between 0 and 1. Even though (A3) is independent of ϕ , it is useful to update this variable in order to increase the rate at which the phase space is sampled. We therefore chose a new ϕ with

$$\phi = 2\pi R_2. \quad (\text{A4})$$

The polar angle θ is instead obtained by

$$\cos \theta = \frac{1}{H} \ln[1 + R_1(e^{2H} - 1)] - 1. \quad (\text{A5})$$

It is important to note that the heat bath method does not rely on an accept-reject approach. Instead, the new

configuration is already generated with the right probability.

When both spins and chiralities are present in the Hamiltonian, the same updating algorithm can be applied to the chiralities. In our simulations, we consecutively chose a random site on the lattice, updated the spin and then the chirality on another random site. Quantities like the energy or the magnetization were usually calculated after N such moves, i.e., after the system had undergone one Monte Carlo step per site on average.

Because we are working with continuous degrees of

freedom and not with discrete variables as in the Ising model for example, the heat bath algorithm is better suited than the conventional Metropolis method. In the Metropolis method, at low temperatures, one starts rejecting many moves because the system prefers to make small fluctuations about local minima of the energy. Thus, it may be very difficult to reach equilibrium or even to know whether one has reached it. By contrast, the heat bath method provides an efficient way to reach the actual minimum of the energy because a new vector orientation is obtained every time, at any temperature.

-
- ¹ See e.g. the review on CuGeO_3 by J.-P. Boucher and L.-P. Regnault, *J. Physique* **6**, 1939 (1996).
- ² E. Dagotto and T.M. Rice, *Science* **271**, 618 (1996).
- ³ R. Melzi, P. Carretta, A. Lascialfari, M. Mambrini, M. Troyer, P. Millet, and F. Mila, *Phys. Rev. Lett.* **85**, 1318 (2000).
- ⁴ H. Kageyama, K. Yoshimura, R. Stern, N.V. Mushnikov, M. Kato, K. Kosuge, C.P. Slichter, T. Goto, and Y. Ueda, *Phys. Rev. Lett.* **82**, 3168 (1999).
- ⁵ K. Kodama, M. Takigawa, M. Horvatić, C. Berthier, H. Kageyama, Y. Ueda, S. Miyahara, F. Becca, and F. Mila, *Science* **298**, 395 (2002).
- ⁶ M. Matsumoto, B. Normand, T.M. Rice, and M. Sigrist, *Phys. Rev. Lett.* **89**, 077203 (2002).
- ⁷ See also, e.g., T.M. Rice, *Science* **298**, 760 (2002).
- ⁸ M.J. Harris, M.P. Zinkin, Z. Tun, B.M. Wanklyn, and I.P. Swainson, *Phys. Rev. Lett.* **73**, 189 (1994); R. Moessner and J.T. Chalker, *Phys. Rev. Lett.* **80**, 2929 (1998).
- ⁹ X. Obradors, A. Labarta, A. Isalgue, J. Tejada, J. Rodriguez, and M. Pernet, *Solid State Commun.* **65**, 189 (1988).
- ¹⁰ A.P. Ramirez, G.P. Espinosa, and A.S. Cooper, *Phys. Rev. Lett.* **64**, 2070 (1990); see also, A. P. Ramirez, *Ann. Rev. Matter. Sci.* **24**, 453 (1994).
- ¹¹ J.T. Tholence, *Physica (Amsterdam)* **126B**, 157 (1984).
- ¹² C. Dekker, A.F.M. Arts, and H.W. de Wijn, *Phys. Rev. B* **38**, 8985 (1988).
- ¹³ P. Chandra, P. Coleman, and I. Ritchey, *J. Phys. I France* **3**, 591 (1993); see also P. Chandra and P. Coleman, *New outlooks and old dreams in quantum antiferromagnets in Strongly interacting fermions and high-temperature superconductivity*, Les Houches Lecture Notes (Session LVI), edited by B. Doucot and J. Zinn-Justin (North-Holland, 1995), p. 495.
- ¹⁴ T. Chalker, P.C.W. Holdsworth, and E.F. Shender, *Phys. Rev. Lett.* **68**, 855 (1992).
- ¹⁵ A.B. Harris, C. Kallin, and A.J. Berlinsky, *Phys. Rev. B* **45**, 2899 (1992).
- ¹⁶ C. Zeng and V. Elser, *Phys. Rev. B* **42**, 8436 (1990).
- ¹⁷ J.T. Chalker and J.F. Eastmond, *Phys. Rev. B* **46**, 14201 (1992).
- ¹⁸ P.W. Leung and V. Elser, *Phys. Rev. B* **47**, 5459 (1993).
- ¹⁹ R.P. Singh and D. Huse, *Phys. Rev. Lett.* **68**, 1766 (1992).
- ²⁰ N. Elstner and A.P. Young, *Phys. Rev. B* **50**, 6871 (1994).
- ²¹ S. Sachdev, *Phys. Rev. B* **45**, 12377 (1992).
- ²² J. Villain, R. Bidaux, J.P. Carton, and R. Conte, *J. Phys. (Paris)* **41**, 1263 (1980).
- ²³ P. Chandra, P. Coleman, and A.I. Larkin, *Phys. Rev. Lett.* **64**, 88 (1989).
- ²⁴ K.H. Fischer and J.A. Hertz, *Spin glasses*, Cambridge University Press (1991).
- ²⁵ K. Binder and A.P. Young, *Rev. Mod. Phys.* **58**, 801 (1986).
- ²⁶ N. Reimers and A. J. Berlinsky, *Phys. Rev. B* **48**, 9539 (1993).
- ²⁷ F. Mila, *Phys. Rev. Lett.* **81**, 2356 (1998).
- ²⁸ F. Mila and D. Dean, *Eur. Phys. J. B* **26**, 301 (2002).
- ²⁹ An effective Hamiltonian, similar to the one of Ref. 27 has been derived for all generic half-integer spins S , and the analysis in this direction is in progress (M. Mambrini, private communication).
- ³⁰ J.A. Olive, A.P. Young, and D. Sherrington, *Phys. Rev. B* **34**, 6341 (1986).
- ³¹ Y.J. Uemura *et al.*, *Phys. Rev. Lett.* **73**, 3306 (1994).